Estuarine, Coastal and Shelf Science 178 (2016) 77–85

Contents lists available at ScienceDirect

Estuarine, Coastal and Shelf Science

journal homepage: www.elsevier.com/locate/ecss

Efficient three-dimensional reconstruction of aquatic vegetation geometry: Estimating morphological parameters influencing hydrodynamic drag

Jean Liénard [a], Kendra Lynn [b], Nikolay Strigul [a], Benjamin K. Norris [c], Demetrios Gatziolis [d], Julia C. Mullarney [c], Karin, R. Bryan [c], Stephen M. Henderson [b, *]

[a] Department of Mathematics and Statistics, Washington State University, Vancouver, WA 98686, USA
[b] School of the Environment, Washington State University, Vancouver, WA 98686, USA
[c] Coastal Marine Group, Faculty of Science and Engineering, University of Waikato, Hamilton, 3240, New Zealand
[d] USDA Forest Service, Pacific Northwest Research Station, Portland, OR 97205, USA

ARTICLE INFO

Article history:
Received 5 October 2015
Received in revised form
27 April 2016
Accepted 11 May 2016
Available online 24 May 2016

Keywords:
Drag coefficient
Photogrammetry
Mangrove
Estuaries
Emergent vegetation
Plant morphology

ABSTRACT

Aquatic vegetation can shelter coastlines from energetic waves and tidal currents, sometimes enabling accretion of fine sediments. Simulation of flow and sediment transport within submerged canopies requires quantification of vegetation geometry. However, field surveys used to determine vegetation geometry can be limited by the time required to obtain conventional caliper and ruler measurements. Building on recent progress in photogrammetry and computer vision, we present a method for reconstructing three-dimensional canopy geometry. The method was used to survey a dense canopy of aerial mangrove roots, called pneumatophores, in Vietnam's Mekong River Delta. Photogrammetric estimation of geometry required 1) taking numerous photographs at low tide from multiple viewpoints around 1 m^2 quadrats, 2) computing relative camera locations and orientations by triangulation of key features present in multiple images and reconstructing a dense 3D point cloud, and 3) extracting pneumatophore locations and diameters from the point cloud data. Step 3) was accomplished by a new 'sector-slice' algorithm, yielding geometric parameters every 5 mm along a vertical profile. Photogrammetric analysis was compared with manual caliper measurements. In all 5 quadrats considered, agreement was found between manual and photogrammetric estimates of stem number, and of number × mean diameter, which is a key parameter appearing in hydrodynamic models. In two quadrats, pneumatophores were encrusted with numerous barnacles, generating a complex geometry not resolved by hand measurements. In remaining cases, moderate agreement between manual and photogrammetric estimates of stem diameter and solid volume fraction was found. By substantially reducing measurement time in the field while capturing in greater detail the 3D structure, photogrammetry has potential to improve input to hydrodynamic models, particularly for simulations of flow through large-scale, heterogenous canopies.

1. Introduction

Regions of aquatic vegetation, such as seagrass beds, saltmarshes and mangrove forests, contribute to biodiversity (Greenberg et al., 2006) while providing ecosystem services (Brander et al., 2006) such as carbon sequestration (Siikamäki et al., 2012) and biogeochemical processing of terrestrial run-off (Gren, 1995). Marine vegetation can shelter coasts from energetic currents, waves (Jadhav et al., 2013) and tsunamis (Alongi, 2008), enhancing coastal stability (Kirwan and Murray, 2007; van Maanen et al., 2015) by reducing erosion (Gacia and Duarte, 2001) or enabling deposition of fine-grain sediments (Furukawa et al., 1997; Bouma et al., 2007). Growing interest in the ability of vegetation to reduce flooding and erosion (Temmerman et al., 2013; Feagin et al., 2015) is further motivated by sea level rise (Nicholls et al., 1999; Arkema et al., 2013), wetland destruction (Thu and Populus, 2007; Giri et al., 2011), and the growth of coastal population

* Corresponding author.
E-mail address: steve_henderson@wsu.edu (S.M. Henderson).

http://dx.doi.org/10.1016/j.ecss.2016.05.011
0272-7714/

centers (Small and Nicholls, 2003). Dissipation of wave and current energy by vegetation canopies depends on plant morphology and density (Temmerman et al., 2005b; Nepf, 2012; Dalrymple et al., 1984). Therefore, morphology and density measurements are required to understand and model the sheltering effects of aquatic vegetation.

Several parameters quantifying canopy morphology are routinely used in models for hydrodynamic drag and associated wave dissipation (Mullarney and Henderson, 2016). One simple and important parameter is the number of plant stems per unit horizontal area of seabed, denoted here by N (units m^{-2}). Elevation-dependent N is defined as the number of stems reaching at least an elevation z above the bed. Another important parameter is the vegetation's mean stem diameter ($\overline{d}$), which can also be evaluated as a function of z. Models for steady flows through rigid vegetation (Nepf, 2012; Temmerman et al., 2005b; Guannel et al., 2015; Belcher et al., 2003) often represent the hydrodynamic drag force F_D per unit volume, which acts to dissipate currents, using the formula

$$F_D = N\overline{d}\, f_1(u,\rho) = a\, f_1(u,\rho), \tag{1}$$

where we have introduced the parameter $a = N\overline{d}$, and the function $f_1(u,\rho)$ represents the dependence of drag on the water velocity u and water density ρ [models typically set $f_1(u,\rho) = (C_D/2)\rho u^2$, where C_D is a dimensionless drag coefficient, often order-one]. It can be shown that a is the cross-sectional area of stems, normal to the water flow direction, per unit volume of canopy (units m^{-1}, Finnigan, 2000). To account for rapid flow accelerations under waves, a widely-used generalization of Eq. (1) is the "Morison equation" $F_D = a\, f_1(u,\rho) + \varphi\, f_2(\partial u/\partial t, \rho)$ (Sumer and Fredsøe, 1997), where φ is the proportion of volume occupied by the solid canopy (for uniform, round stems, $\varphi = N\pi\overline{d}^2/4$, Mullarney and Henderson, 2016), and the function $f_2(\partial u/\partial t, \rho)$ represents the dependence of drag on Eulerian water acceleration $\partial u/\partial t$ and density ($f_2 = C_M\rho\partial u/\partial t$, where t = time and C_M is a dimensionless coefficient, often order-one). Therefore, both a and φ are required by common models for drag under rapidly accelerating flows. However, when calculating wave dissipation for rigid vegetation, it can be shown (e.g. Mullarney and Henderson, 2016) that contributions from the term involving φ average to nearly zero. Therefore, a is a particularly important parameter for modeling both slowly varying currents and higher frequency waves. For flexible vegetation, wave dissipation can be reduced as stems move back and forth with surrounding water (Utter and Denny, 1996; Méndez et al., 1999; Riffe et al., 2011). Models simulating stem motion require knowledge of hydrodynamic parameters and the geometric parameters such as N and $\overline{d}$ considered here, as well as plant material properties, such as the Young's modulus, which are beyond the scope of this paper (Mullarney and Henderson, 2010; Zeller et al., 2014).

Surveys of vegetation geometry have focused on subsamples of the full canopy, with measurements confined to a few small (often 0.1–1 m^2) quadrats (Temmerman et al., 2005b; Lightbody and Nepf, 2006; Riffe et al., 2011; Feagin et al., 2011; Paul and Amos, 2011). Subsampling is necessary because of the very large number of stems present in natural canopies (e.g. millions of stems in 100 × 100 m regions of natural sedge or Spartina saltmarsh, Jadhav et al., 2013; Riffe et al., 2011). For hydrodynamic modeling, subsampling should resolve the vertical variability in canopy geometry. Accurate modeling may also require sampling of lateral variability on scales ranging from meters to kilometers, because such heterogeneity can generate leading-order variability in water flows (Lightbody et al., 2008). Seasonal variability is also observed (Paul and Amos, 2011; Möller, 2006), but is not easily measured by sampling schemes that require the removal of vegetation from the field site (e.g. Lightbody and Nepf, 2006; Feagin et al., 2011; Temmerman et al., 2005a). Unfortunately, logistical constraints on time and labor often preclude sampling of three-dimensional spatial variability in canopy geometry (and possible seasonal variability) using conventional rulers, calipers, and hand counts. Indeed, even sampling a single small quadrat can sometimes be challenging. For example, below we present cases where numerous barnacles growing on stems produced such rough, irregular stem geometry that even sampling a single square meter by caliper measurements would require many hours of fieldwork. To address the challenges resulting from complex geometry of individual stems, and from heterogeneity of larger-scale vegetation statistics, more efficient, automated, non-invasive methods for measuring vegetation geometry are needed.

Analysis of photographic images has been used to estimate morphological characteristics of aquatic vegetation. For one approach (Möller, 2006; Neumeier, 2005; Lemein et al., 2015), a small (e.g. 0.2-m-wide) region of saltmarsh vegetation is isolated while exposed at low tide, a vertical backing board is placed behind the vegetation, and photographs of the horizontal view of the vegetation are analyzed. The percent of the backing board obscured by vegetation, here denoted B, has been related to biomass Neumeier (2005); Möller (2006); Lemein et al. (2015). Within a sedge canopy, a strong correlation has also been found between B and $N\overline{d}h$ (Lemein et al., 2015), where h = stem length (for a uniform-height canopy with depth-independent $\overline{d}$, $N\overline{d}h$ is the depth-integral of a). Vegetation height has been estimated from depth-dependence of B (Möller, 2006; Lemein et al., 2015). Depth-dependence of a has not been inferred directly from photographs, although a profiles have been estimated by combining photogrammetric estimates of stem length with an empirical relationship between stem length and diameter (Lemein et al., 2015, such relationships likely depend on species and seasonality).

This study is motivated by the idea that richer morphological information can be gleaned if multiple photographs, taken from varying angles and locations, are combined using modern photogrammetry techniques. When several 2D photographs are combined, the 3D structure of objects can be determined by triangulation (Hartley and Zisserman, 2004). This approach, often applied to mapping landscapes (Lane et al., 2000; Lejot et al., 2007) and archaeological sites (Brutto and Meli, 2012), has become steadily more efficient with improvements in computational power and computer vision algorithms (Hartley and Zisserman, 2004; Yastikli, 2007; Westoby et al., 2012). Modern automated photogrammetry software (e.g. VisualSfM) allows reconstruction of complex objects from hundreds, or even thousands of photographs. Although vegetation canopies are often more complex and irregular than archaeological artifacts and simple landscapes, recent analyses have demonstrated that photogrammetry can be used to reconstruct complex tree crowns (Gatziolis et al., 2015; Liénard et al., 2016). In the context of aquatic vegetation, reconstructions obtained by combining multiple photographs have been used to determine the stem number density N near the seabed in a pneumatophore canopy (Zhang et al., 2015). However, to our knowledge, the potential of photogrammetry to resolve the full vertical profile of aquatic vegetation geometry has not previously been exploited. Here, multiple photographs taken in the mangrove forests of the Mekong Delta, Vietnam are used to reconstruct the three-dimensional geometry of dense nearbed vegetation.

The major steps in the analysis are summarized in Fig. 1. First, photographs of vegetation were taken in the field from numerous points of view, with substantial overlap (Section 2). Then, a standard photogrammetric approach was used to build a 3D point cloud representing the scene (Section 3). Finally, a geometrical model of the canopy was computed and used to evaluate parameters

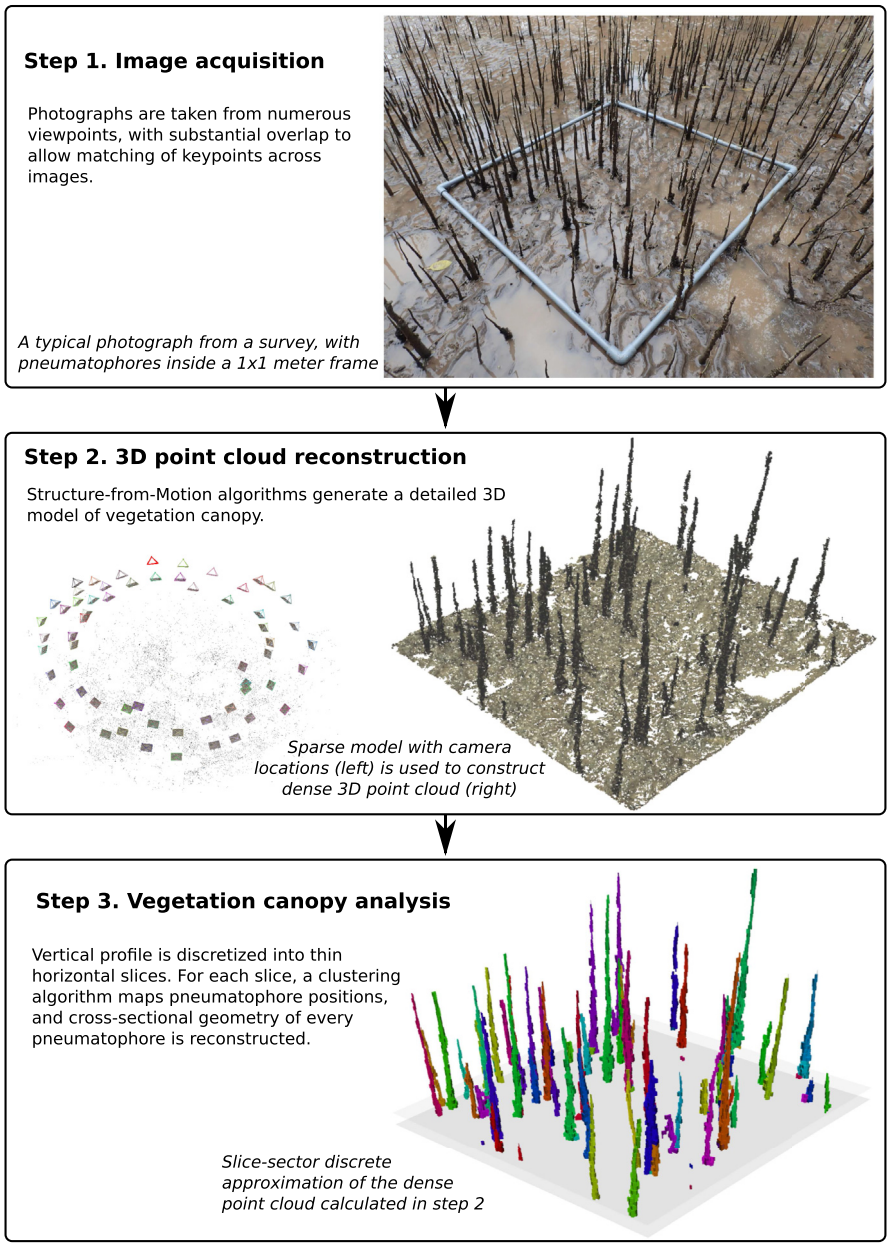

Fig. 1. Overview of the photogrammetry approach to analyze pneumatophore canopy.

required by hydrodynamic models, including N, $\overline{d}$, φ, and a (Section 4). We test photogrammetric parameter estimates by comparison with results obtained by calipers and hand counts (Section 5) and conclude with a brief discussion (Section 6).

2. Field measurements

Field measurements were obtained during September–October 2014, as part of a larger study of hydrodynamics and sediment transport within mangrove forests at the Southern, ocean-exposed shore of Cù Lao Dung Island in the Mekong Delta, Vietnam. The forest is predominantly composed of *Sonneratia caseolaris* trees, and the data presented here focused on the dense canopy of pneumatophore stems that grew upward from the buried lateral roots of trees (median stem heights 0.1–0.25 m).

Vegetation geometry was surveyed at low tide in five 1 m^2 quadrats, each demarcated by a square frame constructed from PVC pipe. Quadrat locations were chosen to encompass a range of pneumatophore densities and sizes. For all stems longer than about 1 cm, ruler and calipers were used to measure stem length along with basal, mid, and tip diameters, respectively at elevations roughly 1 cm, 0.5ℓ, and $\ell - 1$ cm above bed, where ℓ = stem length (elevations for caliper measurements were estimated by eye, and likely deviated from these values by about ±1–3 cm, i.e. about 10% of pneumatophore length). Barnacles, which grew on some pneumatophores, were avoided by making caliper measurements slightly above or below barnacle locations.

For each quadrat, multiple (>55) photographs were taken from various locations and angles (Step 1, Fig. 1). The photographer stood about 1–2 m from the quadrat, taking care not to cast a shadow over the sampled vegetation. Photographs were acquired with a variety of camera orientations, taken while varying the azimuthal

and tilt angles of the camera. Camera pitch varied from nearly horizontal (lateral view, with camera at low elevation) to overhead (oblique view, with raised camera). A minimum of fourteen angular positions were used as the photographer slowly completed a full circle around the quadrat. A standard waterproof digital camera (Olympus TG-3) was used, operating in default mode (automatic focus and exposure) at maximum resolution (16 Megapixels). A photographic survey of a single quadrat could be completed in about 5 min.

3. Reconstruction of 3D point clouds

Three-dimensional point clouds were constructed using the freeware package VisualSfM (Wu, 2011). First, key features were identified across multiple pictures using the SIFT (Scale Invariant Feature Transform Lowe, 2004; Wu, 2007) algorithm. Next, the key features were used to infer camera positions and orientations using Parallel Bundle Adjustment software Wu et al. (2011). Finally, a dense 3D point cloud was reconstructed using the CMVS (Clustering Views for Multi-View Stereo, Furukawa and Ponce, 2010) package. This open-source software generates local surfaces around matched keypoints, and then repeatedly expands these to nearby pixels, based on correspondence between images. Point clouds were cropped in open source software CloudCompare (Girardeau-Montaut, 2011) to remove quadrat frames, and all points outside. Operational details of workflow are given in online supplementary materials.

For each quadrat, about 25–45 min are required to generate vegetation statistics from a set of photographs. Of this time, about 15 min of computer time is required for reconstruction of the three-dimensional point cloud, and most of the remaining time is required to prepare the resultant point cloud for analysis. For comparison, surveying a densely populated quadrat with the traditional hand-count methods may take up to several hours.

4. Vegetation canopy analysis

Although pneumatophores are simple, upright, tapered stems, canopy geometry was sometimes complicated by numerous barnacles growing on the roots. Consequently, conversion of the dense 3D point cloud into estimates of pneumatophore locations and elevation-dependent diameters is challenging. We developed an algorithm, here called the slice-sector approximation, to quantify the complex geometry. The dense point cloud was first split into 5-mm-thick slices corresponding to different elevation ranges (e.g. all points 0.1–0.105 m above bed were treated as one slice). Within each slice, the geometrical properties of the pneumatophores were estimated. To do this, points were first clustered into groups corresponding to individual pneumatophores. Then N was estimated from the number of clusters, and $\overline{d}$ was estimated from a typical cluster diameter. Repeating this process for every 5-mm-thick slice along a vertical profile yielded a 3D reconstruction of the canopy geometry. Operational details of workflow are given in online supplementary materials.

Clustering of the points (Fig. 2a) was achieved using the mean-shift algorithm (Comaniciu and Meer, 2002), performed here with R routines from package LPCM (Einbeck, 2011). For the present application, it is important that the non-parametric mean-shift algorithm requires no prior knowledge of the number of clusters, and does not constrain cluster shape. A critical parameter is the bandwidth h of the Gaussian kernels used to identify clusters (Comaniciu and Meer, 2002). If h is too large (compared to the distance between pneumatophores), then multiple pneumatophores are grouped into one cluster, whereas if h is too small, the point cloud corresponding to an individual pneumatophore is split into several groups. To choose the value of h for results presented below, pneumatophore geometries were repeatedly calculated for values between 2.5 mm and 7.5 mm (using 0.25 mm increments), and the value yielding the most symmetrical pneumatophore models was chosen (minimizing the average ratio of smallest to largest diameter). An alternative approach of simply setting h to 5 mm yielded similar results (not shown).

After points were clustered into groups, the slice-sector approximation was fitted to each group to represent the cross-section of each pneumatophore (Fig. 2b). The pneumatophore center was calculated as the mean location of all points within a cluster, and the pneumatophore was approximated by eight circular sectors radiating from this center. Similar slice-sector geometry has previously been used in spatially explicit, individual-based simulations of forest growth (Strigul, 2012; Liénard and Strigul, 2016). For each pneumatophore, a single stem diameter was calculated as twice the mean of the eight sector radii. Averaging diameters over all stems yielded an estimate of $\overline{d}$. To estimate the solid volume fraction φ, the area enclosed by all sectors of all pneumatophores was summed and divided by the total horizontal area sampled within the quadrat (1 m^2). The slice-sector approximation was evaluated using original R code (available as online supplement to this manuscript), and a Graphical User Interface, GUI, was developed to facilitate ease of use.

5. Comparison between manual and photo-based surveys

The slice-sector methodology provided approximations that visually matched well with the pneumatophore canopy (Figs. 1 and 3). To quantify the accuracy of the 3D photogrammetric reconstructions, we compared the modeled canopy with manual caliper measurements obtained for all five quadrats, labeled Q:a,Q:b,…,Q:e. Photogrammetry quantified pneumatophore diameter every 5 mm along the vertical profile, whereas caliper measurements were obtained at only three elevations (base, middle, and tip) along each pneumatophore. For comparison, the sparse caliper measurements were interpolated to a 5 mm vertical grid by assuming that each pneumatophore's diameter varied linearly between measurement elevations. Errors caused by this interpolation were estimated as shown in Fig. 4, and will be represented by error bars in subsequent figures. Results are summarized in this section, and full vertical profiles of N, $\overline{d}$, and a are given for all quadrats in the Online Supplement.

Manual and photogrammetric estimates of elevation-dependent N were in good agreement (Fig. 5). For each quadrat, one N value was obtained by photogrammetry for every 5 mm slice. For every quadrat, regressing these N values against equivalent caliper-based estimates yielded correlations exceeding 0.95 (Fig. 5a and b). Despite the good agreement between the model and hand counts, discrepancies appear close to the ground for quadrats Q:a and Q:d, as a result of having two touching pneumatophores recognized as one in the slice-sector approximation (Fig. 5, see also Figs. 1 and 2 in the supplementary materials).

Manual and photogrammetric estimates of mean stem diameter $\overline{d}$ and volume fraction φ were also compared (Fig. 6). Errors caused by interpolation of sparse caliper measurements onto a dense vertical grid were substantial. Photogrammetric estimates of $\overline{d}$ were between the min and max estimates obtained using these error bars in 74% of the slices (Fig. 6). The greatest departures were observed in quadrats "Q:c" and "Q:d", where the photo-based estimates fell within the min and max for only 24% of the slices, with large departures at elevations between 0.15 m and 0.3 m (e.g. Fig. 7). Re-examination of photographs revealed particularly dense barnacle growth in these two quadrats and at these elevations (Fig. 7 right). Therefore, this discrepancy likely indicates bias

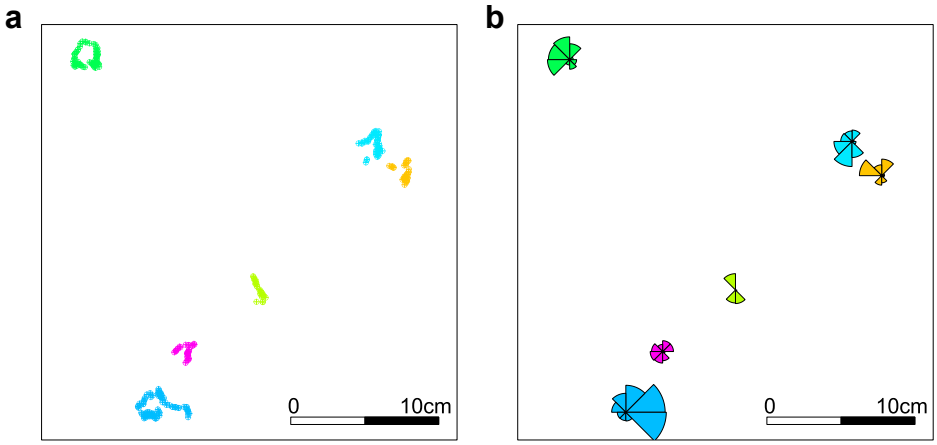

Fig. 2. Illustration of the principal steps of the slice-sector approximation. Panel a: points from one horizontal slice are first clustered to identify one group points with each pneumatophore (each group represented with a different color). Panel b: circular sectors are then computed to approximate the shapes of the pneumatophore cross-sections.

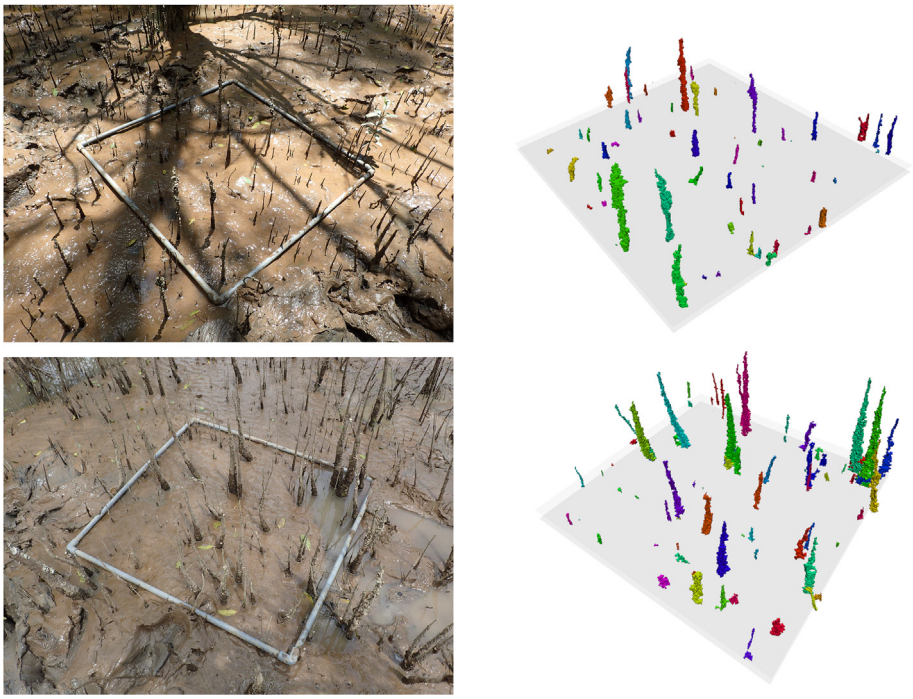

Fig. 3. Photos (left) and corresponding slice-sector approximations (right), taken from similar viewpoints. The quadrats represented are "Q:d" (top) and "Q:e" (bottom).

resulting from a choice to exclude barnacles from caliper measurements (Section 2). After excluding quadrats Q:c and Q:d, most remaining large discrepancies between photogrammetric and caliper estimates were based on small samples sizes (small N values), usually obtained at high elevations reached by only a few pneumatophores (open symbols in Fig. 6). The cases with few pneumatophores were associated with such small φ values that open symbols in Fig. 6b, although plotted, are difficult to distinguish from zero. After removing both quadrats Q:c and Q:d and small sample sizes, 90% of diameters obtained by photogrammetry were between min and max values estimated from caliper measurements. Nevertheless, the range between min and max values was large, and agreement between photogrammetric and caliper estimates was less clear for $\overline{d}$ than for N.

The parameter a is vital to models for the fluid drag exerted by pneumatophores (Eq. (1)). Vertical profiles of a estimated from photogrammetric surveys and hand counts were in good agreement (Fig. 8a). Specifically, 71% of the within-slice frontal area estimates fell between the min and max values inferred from caliper measurements. The dimensionless depth-integral of a (sometimes denoted λ_f, Britter and Hanna, 2003) evaluated by photogrammetry fell between the min and max values inferred from manual surveys for all quadrats (Fig. 8b).

6. Discussion

We have developed and tested a photogrammetric technique to quantify the three-dimensional structure of aquatic vegetation. For the mangrove pneumatophore canopy considered, high quality estimates of N and a were obtained every 5 mm along a vertical profile, whereas estimates of $\overline{d}$ and φ were of moderate quality. The ability of photogrammetric analysis to efficiently measure vertical

Fig. 4. Illustration of the error bounds for manual measurements. Diameters were measured at three locations: basal, middle and top. These measurements were linearly interpolated to estimate stem diameters at all elevations (solid lines). Upper and lower bounds on diameter were obtained by neglecting taper between measurement elevations (dotted vertical lines). In this particular example, the true diameter lies in between the "linear" and the "min" estimates, but in some other cases (not shown) the true diameter was between "linear" and "max" estimates.

researchers (e.g. Mazda et al., 2006), of pneumatophores to near-bed flows.

The 3D point clouds produced here as an intermediate step in photogrammetric analysis resemble the point clouds produced by scanning LiDAR (Côté et al., 2009; Gatziolis et al., 2010; Calders et al., 2015). Although LiDAR may provide more accurate data in some cases, photogrammetric analysis was sufficient to resolve the pneumatophore canopy of ~1-cm-diameter stems analyzed here. Unlike scanning LiDAR, the handheld cameras used here are compact, lightweight, shockproof, waterproof, and cheap.

Photogrammetry has several advantages over manual surveys and caliper measurements. Photogrammetry is more time efficient, making more extensive surveys feasible. This time efficiency of photogrammetry is likely to improve further with future technological advances. Furthermore, photogrammetry can resolve complex geometries, such as barnacle-encrusted pneumatophores, that would be extremely difficult to measure with calipers. The manual diameter measurements used for method validation excluded barnacles. For cases with abundant barnacles, substantial discrepancies between manual and photo-based surveys resulted (Fig. 7). Unlike most hand counts, photogrammetry also locates stems in 3D space, a capability that could be useful for construction of stem-resolving numerical flow simulations (c.f. Kaandorp et al., 2003).

Although the techniques developed here adequately resolved the pneumatophore canopy considered, challenges might arise if more complex vegetation canopies were reconstructed. The slice-sector approximation may perform poorly if used to represent very flattened objects such as leaves. In cases with a very wide range of stem diameters (e.g. regions containing both tree trunks and pneumatophores) it might prove difficult to find a bandwidth appropriate for all stems, and consequently some alternative clustering algorithm may be required. The height of slices, here set to 5 mm, can also affect results: slices that are too thin may contain insufficient points for reconstruction, whereas slices that are too

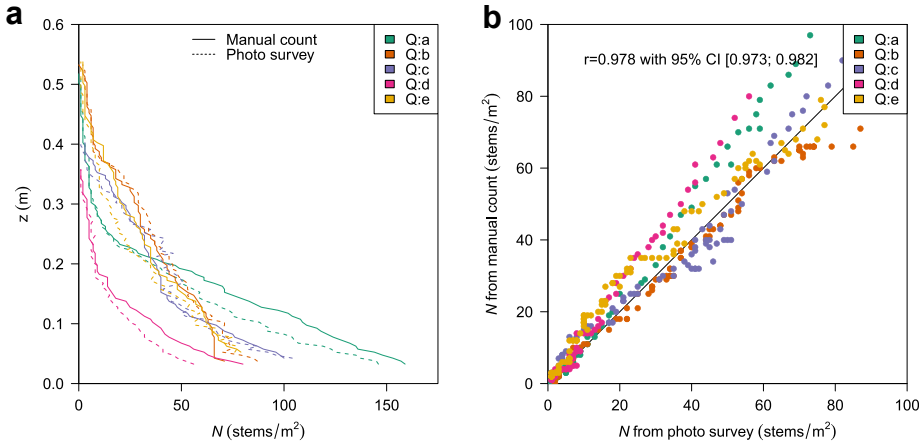

Fig. 5. Number of stems determined by hand counts and by photogrammetry. Panel a: stem counts as a function of height. Panel b: scatter plot of photo vs manual counts (each dot represents one 5 mm slice).

profiles of *a* is particularly relevant to hydrodynamic models, which often assume that vegetation drag and wave dissipation are proportional to *a* (Section 1). Consistent with previous observations of similar mangroves (*Sonneratia* sp., Mazda et al., 2006; Zhang et al., 2015), observed *a* values reached about 1 m^{-1} near the bed, about two orders of magnitude larger than values often associated with mangrove trunks above the pneumatophore canopy (Mazda et al., 2006). This highlights the importance, noted by previous

thick lead to overestimation of stem diameter. Such overestimation indicates that some points within clusters are far from cluster centers, either because of real within-slice variations in diameter (possibly owing to barnacles), or because of errors in the 3D point cloud (a few large errors are expected given sufficiently thick slices). For this application, good results were obtained for slice thickness between 2 and 10 mm (not shown). The analysis presented here also requires that the vegetation remains still during

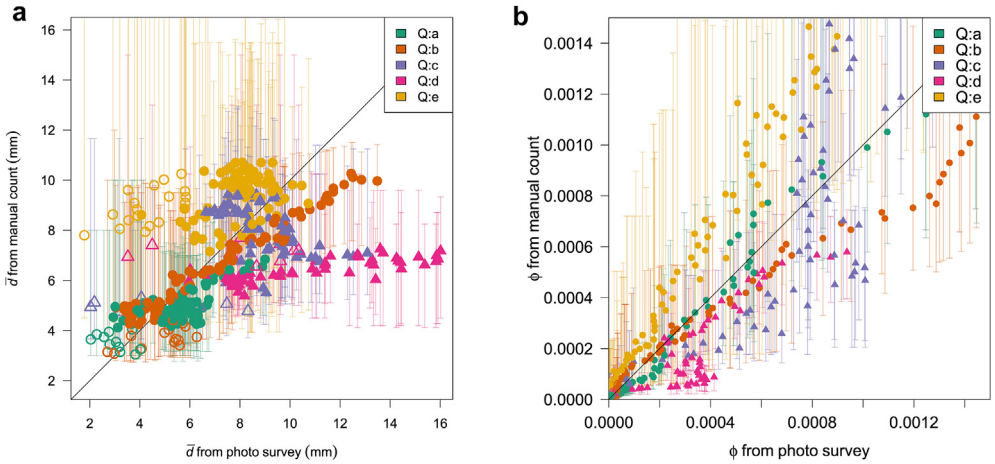

Fig. 6. Comparison of diameters (panel a) and pneumatophore volume fraction (panel b) between manual measurements and photo-based surveys. The error bars represent uncertainty in diameters resulting from interpolation of manual measurements (Fig. 4). Triangles and circles, respectively, mark quadrats with (Q:c and Q:d) and without (Q:a, Q:b, Q:e) numerous barnacles. Empty symbols indicate the 10% of slices with the fewest pneumatophores, whereas filled symbols indicate slices with larger samples of pneumatophores.

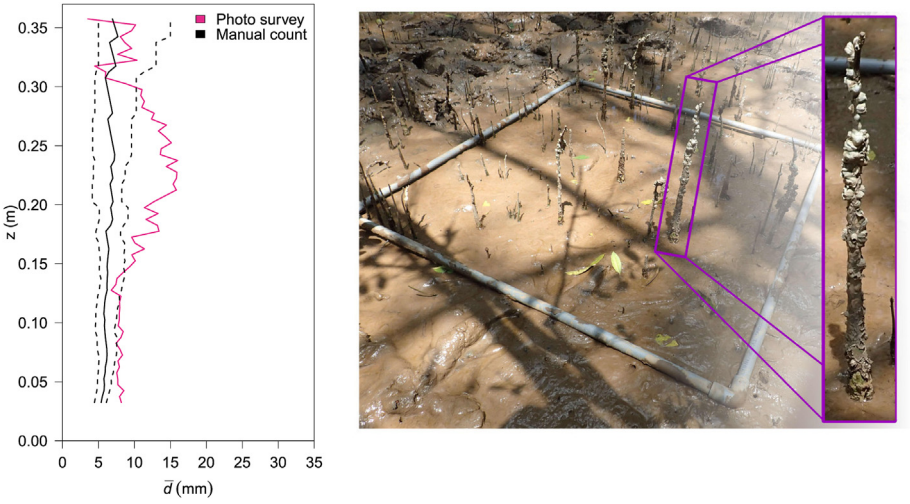

Fig. 7. Influence of barnacles on estimated mean diameter, Quadrat Q:d. Difference between photographic (pink) and manual (black, with dashed lines showing uncertainty) diameter estimates (left) can be explained by presence of numerous barnacles (center, right), which were excluded from manual measurements but included in the photo survey.

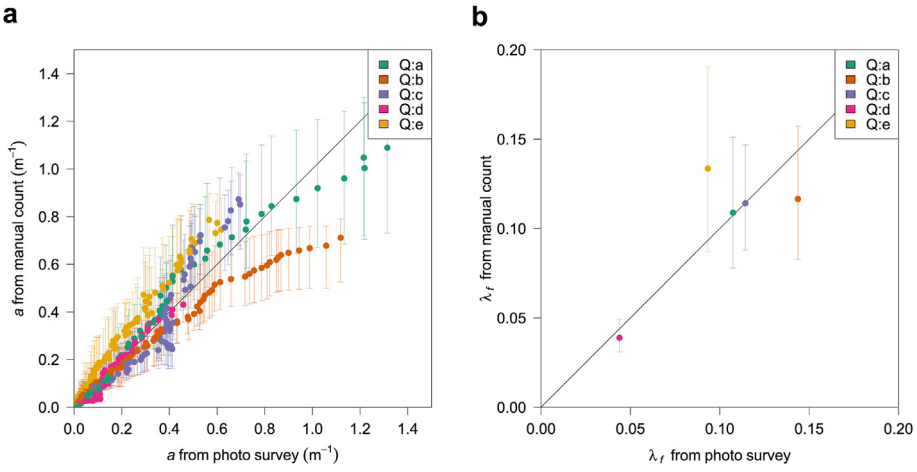

Fig. 8. Frontal area a, evaluated every 5 mm along the vertical profile (panel a), and $\lambda_f = \int a\, dz$ (panel b).

the photographic survey, a condition that may be violated if winds are strong, or if vegetation is very flexible (as is often true for leaves). Movement of shadows cast by overhead vegetation may also degrade results, particularly in windy conditions. In a very dense canopy, views of the canopy interior may be obscured (for square quadrats, obtaining a large sample of stems from a single reconstruction requires $\varphi \ll 1$, because lateral views are obscured over a length scale a^{-1}, so photographs can image stems in an area of order a^{-2}, and the resolvable number of stems is $Na^{-2} \sim \varphi^{-1}$). Finally, although good results were obtained here using 55 or more photographs of each quadrat, all with 16 MP resolution, results would be expected to degrade given fewer photographs or lower resolution. Practical strategies to improve 3D reconstructions include (a) taking a large number of high-definition photographs, and (b) performing automated quality control in real-time (Liénard et al., 2016). Despite the potential challenges, image-based reconstructions already have substantial advantages over conventional methods for the cases tested here, and in coming years further advances can be expected given the ongoing rapid development of computer vision algorithms.

Acknowledgements

During fieldwork in Vietnam, vital logistical support was provided by Huong Phuoc Vu Luong, Charles Nittrouer, Richard Nguyen, Andrea Ogston, and Daniel Culling. Further assistance at the field site was provided by Dean Sandwell, Aaron Fricke, Daniel Culling, Sergio Fagherazzi, William Nardin, Xuan Tien Nguyen Vinh, and Hoang Phong Nguyen. Fieldwork was funded by the US Office of Naval Research, Littoral Geosciences grant number N000141410112, and the Office of Naval Research Global grant number N62909-14-1-N028. Nikolay Strigul funded by a grant from the Simons Foundation (#283770). Kendra Lynn funded by the US National Science Foundation, REU grant number DBI 14-61057. We thank the anonymous reviewer for their helpful suggestions.

Appendix A. Supplementary data

Supplementary data related to this article can be found at http://dx.doi.org/10.1016/j.ecss.2016.05.011.

References

Alongi, D.M., 2008. Mangrove forests: resilience, protection from tsunamis, and responses to global climate change. Estuar. Coast. Shelf Sci. 76 (1), 1–13.
Arkema, K.K., Guannel, G., Verutes, G., Wood, S.A., Guerry, A., Ruckelshaus, M., Kareiva, P., Lacayo, M., Silver, J.M., 2013. Coastal habitats shield people and property from sea-level rise and storms. Nat. Clim. Change 3 (10), 913–918.
Belcher, S., Jerram, N., Hunt, J., 2003. Adjustment of a turbulent boundary layer to a canopy of roughness elements. J. Fluid Mech. 488, 369–398.
Bouma, T.J., van Duren, L.A., Temmerman, S., Claverie, T., Blanco-Garcia, A., Ysebaert, T., Herman, P.M.J., 2007. Spatial flow and sedimentation patterns within patches of epibenthic structures: combining field, flume and modelling experiments. Cont. Shelf Res. 27 (8), 1020–1045.
Brander, L., Florax, R.J., Vermaat, J.E., 2006. The empirics of wetland valuation: a comprehensive summary and a meta-analysis of the literature. Environ. Resour. Econ. 33, 223–250.
Britter, R., Hanna, S., 2003. Flow dispersion in urban areas. Ann. Rev. Fluid Mech. 35, 469–496.
Brutto, M., Meli, P., 2012. Computer vision tools for 3d modelling in archaeology. Int. J. Herit. Digit. Era 1 (Suppl. 1), 1–6.
Calders, K., Newnham, G., Burt, A., Murphy, S., Raumonen, P., Herold, M., Culvenor, D., Avitabile, V., Disney, M., Armston, J., et al., 2015. Nondestructive estimates of above-ground biomass using terrestrial laser scanning. Methods Ecol. Evol. 6 (2), 198–208.
Comaniciu, D., Meer, P., 2002. Mean shift: a robust approach toward feature space analysis. Pattern Anal. Mach. Intell. IEEE Trans. 24 (5), 603–619.
Côté, J.-F., Widlowski, J.-L., Fournier, R.A., Verstraete, M.M., 2009. The structural and radiative consistency of three-dimensional tree reconstructions from terrestrial lidar. Remote Sens. Environ. 113 (5), 1067–1081.
Dalrymple, R., Kirby, J., Hwang, P., 1984. Wave diffraction due to areas of energy dissipation. J. Waterw. Port, Coast. Ocean Eng. ASCE 110 (1), 67–79.
Einbeck, J., 2011. Bandwidth selection for mean-shift based unsupervised learning techniques: a unified approach via self-coverage. J. Pattern Recognit. Res. 6 (2), 175–192.
Feagin, R.A., Figlus, J., Zinnert, J.C., Sigren, J., Martinez, M.L., Silva, R., Smith, W.K., Cox, D., Young, D.R., Carter, G., 2015. Going with the flow or against the grain? the promise of vegetation for protecting beaches, dunes, and barrier islands from erosion. Front. Ecol. Environ. 13, 203–210.
Feagin, R.A., Irish, J., Möller, I., Williams, A., Colon-Rivera, R., Mousavi, M., 2011. Short communication: engineering properties of wetland plants with application to wave attenuation. Coast. Eng. 58, 251–255.
Finnigan, J., 2000. Turbulence in plant canopies. Annu. Rev. Fluid Mech. 32, 519–571.
Furukawa, K., Wolanski, E., Mueller, H., 1997. Currents and sediment transport in mangrove forests. Estuar. Coast. Shelf Sci. 44 (3), 301–310.
Furukawa, Y., Ponce, J., 2010. Accurate, dense, and robust multiview stereopsis. Pattern Anal. Mach. Intell. IEEE Trans. 32 (8), 1362–1376.
Gacia, E., Duarte, C., 2001. Sediment retention by a mediterranean *Posidonia oceanica* meadow: the balance between deposition and resuspension. Estuar. Coast. Shelf Sci. 52 (4), 505–514.
Gatziolis, D., Liénard, J.F., Vogs, A., Strigul, N.S., 2015. 3d tree dimensionality assessment using photogrammetry and small unmanned aerial vehicles. PloS One 10 (9), e0137765.
Gatziolis, D., Popescu, S., Sheridan, R., Ku, N., 2010. Evaluation of terrestrial lidar technology for the development of local tree volume equations. In: Proceedings of SilviLaser, pp. 197–205.
Girardeau-Montaut, D., 2011. Cloudcompare-open source project. OpenSource Project.
Giri, C., Ochieng, E., Tieszen, L.L., Zhu, Z., Singh, A., Loveland, T., Masek, J., Duke, N., 2011. Status and distribution of mangrove forests of the world using earth observation satellite data. Glob. Ecol. Biogeogr. 20 (1), 154–159.
Greenberg, R., Maldonado, J.E., Droege, S., Mcdonald, M.V., 2006. Tidal marshes: a global perspective on the evolution and conservation of their terrestrial vertebrates. Bioscience 56 (8), 675–685.
Gren, I.-M., 1995. The value of investing in wetlands for nitrogen abatement. Eur. Rev. Agric. Econ. 22, 157–172.
Guannel, G., Ruggiero, P., Faries, J., Arkema, K., Pinsky, M., Gelfenbaum, G., Guerry, A., Kim, C.-K., 2015. Integrated modeling framework to quantify the coastal protection services supplied by vegetation. J. Geophys. Res. 120, 324–345. http://dx.doi.org/10.1002/2014JC009821.
Hartley, R.I., Zisserman, A., 2004. Multiple View Geometry in Computer Vision, second ed. Cambridge University Press, ISBN 0521540518.
Jadhav, R.S., Chen, Q., Smith, J.M., 2013. Spectral distribution of wave energy dissipation by salt marsh vegetation. Coast. Eng. 77, 99–107.
Kaandorp, J.A., Koopman, E.A., Sloot, P.M., Bak, R.P., Vermeij, M.J., Lampmann, L.E., 2003. Simulation and analysis of flow patterns around the scleractinian coral *Madracis mirabilis* (Duchassiang and Michelotti. Philos. Trans. R. Soc. Lond. B 358, 1551–1557.
Kirwan, M.L., Murray, A.B., 2007. A coupled geomorphic and ecological model of tidal marsh evolution. Proc. Natl. Acad. Sci. U. S. A. 104 (15), 6118–6122.
Lane, S., James, T., Crowell, M., 2000. Application of digital photogrammetry to complex topography for geomorphological research. Photogramm. Record 16 (95), 793–821.
Lejot, J., Delacourt, C., Piegay, H., Fournier, T., Tremelo, M.-L., Allemand, P., 2007. Very high spatial resolution imagery for channel bathymetry and topography from an unmanned mapping controlled platform. Earth Surf. Process. Landf. 32 (11), 1705–1725.
Lemein, T., Cox, D., Albert, D., Mori, N., 2015. Accuracy of optical image analysis compared to conventional vegetation measurements for estimating morphological features of emergent vegetation. Estuar. Coast. Shelf Sci. 155, 66–74.
Liénard, J., Strigul, N., 2016. An individual-based forest model links canopy dynamics and shade tolerances along a soil moisture gradient. R. Soc. Open Sci. 3 (2).
Liénard, J., Vogs, A., Gatziolis, D., Strigul, N., 2016. Embedded, real-time UAV control for improved, image-based 3D scene reconstruction. Measurement 81, 264–269.
Lightbody, A.F., Avener, M.E., Nepf, H.M., 2008. Observations of short-circuiting flow paths within a free-surface wetland in Augusta, Georgia, USA. Limnol. Oceanogr. 53 (3), 1040–1053.
Lightbody, A.F., Nepf, H.M., 2006. Prediction of velocity profiles and longitudinal dispersion in emergent salt marsh vegetation. Limnol. Oceanogr. 51, 218–228.
Lowe, D.G., 2004. Distinctive image features from scale-invariant keypoints. Int. J. Comput. Vis. 60 (2), 91–110.
Mazda, Y., Magi, M., Ikeda, Y., Kurokawa, T., Asano, T., 2006. Wave reduction in a mangrove forest dominated by sonneratia sp. Wetl. Ecol. Manag. 14, 365–378.
Méndez, F.J., Losada, I.J., Losada, M.A., 1999. Hydrodynamics induced by wind waves in a vegetation field. J. Geophys. Res. Oceans 104 (C8), 18383–18396.
Möller, I., 2006. Quantifying saltmarsh vegetation and its effect on wave height dissipation: results from a UK east coast saltmarsh. Estuar. Coast. Shelf Sci. 69, 337–351.
Mullarney, J.C., Henderson, S.M., 2010. Wave-forced motion of submerged single stem vegetation. J. Geophys. Res. 115 http://dx.doi.org/10.1029/2010JC006448.
Mullarney, J.C., Henderson, S.M., 2016. Flows within marine vegetation canopies. In: Advances in Coastal Hydraulics (under revision).
Nepf, H.M., 2012. Flow and transport in regions with aquatic vegetation. Annu. Rev.

Fluid Mech. 44, 123–142.
Neumeier, U., 2005. Quantification of vertical density variations of salt-marsh vegetation. Estuar. Coast. Shelf Sci. 63 (4), 489–496.
Nicholls, R., Hoozemans, F., Marchand, M., 1999. Increasing flood risk and wetland losses due to global sea-level rise: regional and global analyses. Glob. Environ. Change Hum. Policy Dimens. 9 (Suppl. 1), S69–S87.
Paul, M., Amos, C., 2011. Spatial and seasonal variation in wave attenuation over Zostera noltii. J. Geophys. Res. Oceans 116 (C8). http://dx.doi.org/10.1029/2010JC006797 (1978–2012).
Riffe, K.C., Henderson, S.M., Mullarney, J.C., 2011. Wave dissipation by flexible vegetation. Geophys. Res. Lett. 38 http://dx.doi.org/10.1029/2011GL048773.
Siikamäki, J., Sanchirico, J.N., Jardine, S.L., 2012. Global economic potential for reducing carbon dioxide emissions from mangrove loss. Proc. Natl. Acad. Sci. U. S. A. 109 (36), 14369–14374.
Small, C., Nicholls, R., 2003. A global analysis of human settlement in coastal zones. J. Coast. Res. 19 (3), 584–599.
Strigul, N., 2012. Individual-based models and scaling methods for ecological forestry: implications of tree phenotypic plasticity. In: Garcia, J., Casero, J. (Eds.), Sustainable Forest Management. InTech, Rijeka, Croatia, pp. 359–384.
Sumer, B., Fredsøe, J., 1997. Hydrodynamics Around Cylindrical Structures. Advanced Series in Applied Physics. World Scientific.
Temmerman, S., Bouma, T., Govers, G., Lauwaet, D., 2005a. Flow paths of water and sediment in a tidal marsh: relations with marsh developmental stage and tidal inundation height. Estuaries 28 (3), 338–352.
Temmerman, S., Bouma, T., Govers, G., Wang, Z., De Vries, M., Herman, P., 2005b. Impact of vegetation on flow routing and sedimentation patterns: three-dimensional modeling for a tidal marsh. J. Geophys. Res. Earth Surf. 110 (F4).
Temmerman, S., Meire, P., Bouma, T.J., Herman, P.M.J., Ysebaert, T., De Vriend, H.J., 2013. Ecosystem-based coastal defence in the face of global change. Nature 504 (7478), 79–83.
Thu, P.M., Populus, J., 2007. Status and changes of mangrove forest in Mekong Delta: case study in Tra Vinh, Vietnam. Estuar. Coast. Shelf Sci. 71 (1–2), 98–109.
Utter, B.D., Denny, M.W., 1996. Wave-induced forces on the giant kelp *Macrocystis pyrifera* (AGARDH): field test of a computational model. J. Exp. Biol. 199, 2645–2654.
van Maanen, B., Coco, G., Bryan, K.R., 2015. On the ecogeomorphological feedbacks that control tidal channel network evolution in a sandy mangrove setting. Proc. R. Soc. Lond. A Math. Phys. Eng. Sci. 471 (2180).
Westoby, M., Brasington, J., Glasser, N., Hambrey, M., Reynolds, J., 2012. structure-from-motion photogrammetry: a low-cost, effective tool for geoscience applications. Geomorphology 179, 300–314.
Wu, C., 2007. Siftgpu: a GPU Implementation of Scale Invariant Feature Transform (Sift).
Wu, C., 2011. Visualsfm: a Visual Structure from Motion System. 9.
Wu, C., Agarwal, S., Curless, B., Seitz, S.M., 2011. Multicore bundle adjustment. In: Computer Vision and Pattern Recognition (CVPR), 2011 IEEE Conference on. IEEE, pp. 3057–3064.
Yastikli, N., 2007. Documentation of cultural heritage using digital photogrammetry and laser scanning. J. Cult. Herit. 8 (4), 423–427.
Zeller, R.B., Weitzman, J.S., Abbett, M.E., Zarama, F.J., Fringer, O.B., Koseff, J.R., 2014. Improved parameterization of seagrass blade dynamics and wave attenuation based on numerical and laboratory experiments. Limnol. Oceanogr. 59 (1), 251–266.
Zhang, X., Chua, V.P., Cheong, H.-F., 2015. Geometrical and material properties of *Sonneratia alba* mangrove roots. Trees 29, 285–297.